JOURNAL OF AGRICULTURAL AND FOOD CHEMISTRY

pubs.acs.org/JAFC Article

Crystal Structure and Regiospecificity of Catechol *O*-Methyltransferase from *Niastella koreensis*

Seul Hoo Lee,[#] Bongsang Kim,[#] and Kyung-Jin Kim*

Cite This: *J. Agric. Food Chem.* 2021, 69, 2531−2538 Read Online

ACCESS | Metrics & More | Article Recommendations

ABSTRACT: Catechol *O*-methyltransferase (COMT) is an enzyme that transfers a methyl group to the catechol-derivative substrates using *S*-adenosyl-l-methionine (SAM) and Mg^{2+}. We report the biochemical and structural analysis of COMT from *Niastella koreensis* (*Nk*COMT). *Nk*COMT showed the highest activity with Mg^{2+}, although the enzyme also showed a significant level of activity with Cu^{2+} and Zn^{2+}. *Nk*COMT structures complexed with SAH and Mg^{2+} elucidated how the enzyme stabilized the cosubstrate and the metal ion and revealed that the region near the SAM binding site undergoes conformational changes upon the binding of the cosubstrate and the metal ion. We also identified the catechol binding pocket of the enzyme and explained a broad substrate specificity of the bacterial enzyme and its ability to accommodate the catechol derivatives. In addition, we developed the *Nk*COMT^{E211R} and *Nk*COMT^{E211K} variants that showed both enhanced activities and regiospecificity for the production of the para-forms. Our study provides a structural basis for regiospecificity of *Nk*COMT, which is related with the conformational change upon binding of SAM and Mg^{2+}.

KEYWORDS: *catechol O-methyltransferase, Niastella koreensis, S-adenosyl-l-methionine, regiospecificity*

Downloaded via UNIV OF PRINCE EDWARD ISLAND on May 15, 2021 at 10:35:50 (UTC).
See https://pubs.acs.org/sharingguidelines for options on how to legitimately share published articles.

INTRODUCTION

O-methyltransferases (OMTs) are abundant in biosynthetic pathways of a diverse range of natural products.[1,2] OMTs are divided into classes I and II, and catechol OMT (COMT) belongs to class I OMTs, which have a shorter amino acid sequence than class II OMTs.[3−5] COMT enzymes catalyze the methyl transfer to the catechol compounds and use metal ions and *S*-adenosyl-l-methionine (SAM) as a methyl-donor substrate.[6] COMTs are abundantly distributed in most of the organisms, including bacteria, plants, fungi, and animals.[7−13] X-ray structures of COMT enzymes from both eukaryotic and prokaryotic sources have been solved, and there are various studies on the sequences, structural features, and functions.[14−20] Mammalian COMTs have two isoforms (soluble and membrane-anchored forms) and play important roles in the metabolism of catecholamine neurotransmitters and catechol estrogens.[13,21] Plant COMTs mostly use caffeoyl-CoA, a precursor of the important building blocks in lignin biosynthesis, as a substrate.[22] The application of this COMT enzyme has been studied for the generation of vanillin, one of the most widely used as food additives.[5,23,24] One of the ways to produce vanillin is through a two-step reaction of hydroxylation and methylation from protocatechuate, an intermediate product of various aromatic compounds.[23,24] COMT protein plays a key role in vanillin production through reaction of methylation.

The reaction mechanism and para/meta-regiospecificity of COMT were defined previously.[20,25] These biochemical studies have been conducted in a considerably narrow range, and the tendency has not been predicted as it is too diverse, especially in the case of bacterial COMTs. Because the bacterial COMTs have a broad substrate specificity, they are expected to be involved in various metabolic processes of the aromatic ring compounds such as antibiotics.[5,12,26−29] The para- and meta-selectivities are also different among organisms, such as mammals and plants. Several mutational studies based on the structure of COMTs have been attempted to determine the rules of para- or meta-selectivity.[30,31] However, the preference for its regioselectivity and substrate selectivity is not well-determined yet.[7]

Most of the COMTs are known to utilize Mg^{2+} for enzyme catalysis, and the replacement of the metal ion sometimes results in inexplicable changes in enzyme activity.[32−34] However, detailed investigations on how other metal ions affect enzyme activity have not been conducted yet.

In this paper, we analyzed the biochemical properties of bacterial COMT from the soil bacterium *Niastella koreensis* (*Nk*COMT) and determined its structures in three different forms, an apo, complexed with SAM, and complexed with SAH and Mg^{2+}. Based on structural information, we identified each binding mode of SAM and Mg^{2+}. We revealed that the protein undergoes conformational changes upon the binding of the cosubstrate and the metal ion. We also identified the catechol binding mode of *Nk*COMT and developed its variants showing enhanced regiospecificity against the para-form of the product.

Received: December 3, 2020
Revised: January 28, 2021
Accepted: February 2, 2021
Published: February 17, 2021

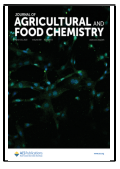

ACS Publications © 2021 American Chemical Society

https://dx.doi.org/10.1021/acs.jafc.0c07621
J. Agric. Food Chem. 2021, 69, 2531−2538

MATERIALS AND METHODS

Enzyme Expression and Purification of *Nk*COMT. The expression and purification of *Nk*COMT were performed by following the published protocols with some changes.[35,36] In brief, we purchased the *Niastella koreensis* strain from Korean Collection for Type Cultures (KCTC, Republic of Korea). The *Nk*COMT gene was amplified by polymerase chain reaction (PCR) and subcloned into a pET30a expression vector by NdeI and XhoI restriction sites. An *Escherichia coli* BL21(DE3)-T1^{R} strain transformed with the pET30a:*Nk*COMT vector was grown to an OD_{600} of 0.7 in an LB medium containing 50 mg/L kanamycin at 312 K, and protein expression was induced by 0.5 mM 1-thio-β-D-galatopyranoside (IPTG) followed by further incubation for 20 h at 293 K. The enzyme purification was performed using a Ni-NTA agarose column (Qiagen) and size-exclusion chromatography using a Sephacryl S-300 column (320 mL, GE Healthcare). The purified protein was concentrated to 37 mg/mL using a concentrator (Amicon Ultra Centrifugal Filter, 10 kDa pore size). All purification procedures were performed at 277 K.

Thermal Stability Detection of *Nk*COMT. Thermal stability of *Nk*COMT with various metal ions was measured by melting curves with a protein thermal shift dye (Applied Biosystems) in StepOnePlus Real-Time PCR (Thermo Fisher Scientific) according to manufacturer's instructions. *Nk*COMT (1 mg/mL, 20 μM) was incubated with each of 1 mM metal ions (Mg^{2+}, Ca^{2+}, Mn^{2+}, Fe^{2+}, Ni^{2+}, Cu^{2+}, Zn^{2+}, Co^{2+}, and Cd^{2+}) for 1 h at 277 K. The reaction mixture contained 5 μg of the metal ion-protein, 1 × protein thermal shift dye (Applied Biosystems), and 2 M Tris-HCl pH 8.0 in 20 μL. *Nk*COMT protein denaturation signals were detected by increasing temperature from 298 to 372 K. Melting temperatures were determined from the first derivative curve.

HPLC Analysis of *Nk*COMT Reaction Products. The reaction samples were analyzed using a CMB-20A HPLC (Shimadzu), equipped with a UV/Vis detector (SPD-20A) and a C18 column (Shimadzu Shim-pack GIS ODS-I C18, 5 μm, 4.6 × 150 mm). Mobile phase A consisted of water containing 0.1% formic acid, and mobile phase B was 100% acetonitrile. The flow rate was 1.5 mL/min for 4 min and changed to 2 mL/min from 4 to 12 min and 50 s followed by 1 mL/min. Mobile phases were as follows: 0−8 min and 50 s, 5% B; 8 min and 50 s−10 min and 30 s, 6% B; 10 min and 30 s−17 min and 50 s, 7.5% B; 17 min and 50 s−21 min, 20% B; 21−23 min, 15% B; 23−27 min, 22% B; 27−29 min, 20% B; 29−40 min, 100% B. Vanillic acid and *iso*-vanillic acid were detected at 280 nm. All experiments were performed in duplicate at a column temperature of 323 K.

Site-Directed Mutagenesis. The forward primers for *Nk*COMT^{E211R} and *Nk*COMT^{E211K} were 5′-ATGGTAGGTGTAAAAAGATACGATGGAATGGCT-3′ (nucleotide 616−648, forward) and 5′-ATGGTAGGTGTAAAAAAATACGATGGAATGGCT-3′ (nucleotide 616−648, forward). The reverse primers for *Nk*COMT^{E211R} and *Nk*COMT^{E211K} were 5′-AGCCATTCCATCGTATCTTTTTACACCTACCAT-3′ (nucleotide 616−648, reverse) and 5′-AGCCATTCCATCGTATTTTTTTACACCTACCAT-3′ (nucleotide 616−648, reverse), respectively. Site-specific mutations were constructed using a QuikChange kit (Stratagene), and sequencing was performed to confirm correct incorporation of the mutations. Mutant proteins were purified with the same method with wild-type *Nk*COMT.

Crystallization of *Nk*COMT. For crystallization screening, commercial crystal-screening kits were used, including Index, PEG ion I and II (Hampton Research), and Wizard Classic I and II (Rigaku Reagents), using the sitting-drop vapor diffusion method with an MRC crystallization plate (Molecular Dimensions) at 295 K that was published in previous paper.[35,36] The apo *Nk*COMT crystals of the best quality appeared in 16% PEG3350 and 8% Tacsimate pH 6.0. The crystallization screening of *Nk*COMT in complex with *S*-adenosyl-l-methionine (SAM) was performed in the same method as apo *Nk*COMT, except for the addition of 10 mM SAM to the protein solution. The crystals of the best quality appeared in 20% PEG4000, 20% 2-propanol, and 0.1 M sodium citrate pH 5.6 supplemented with 10 mM SAM. The crystallization screening of *Nk*COMT in complex with *S*-adenosyl-L-homocysteine (SAH) and Mg^{2+} was performed in the same method as apo *Nk*COMT, except for the addition of 5 mM SAH and 10 mM Mg^{2+} to the protein solution. The crystals of the best quality appeared in 18% PEG8000, 0.1 M MES/sodium hydroxide pH 6.0, and 0.2 M calcium acetate supplemented with 5 mM SAH and 10 mM Mg^{2+}.

Data Collection and Structure Determination of *Nk*COMT. The *Nk*COMT crystals of the best quality were transferred to cryoprotectant solution containing 25% (v/v) glycerol. The crystals were harvested with a loop of 0.2 mm diameter and flash-frozen in a nitrogen gas stream at 100 K. X-ray diffraction data were collected at the 7A beamline of the Pohang Accelerator Laboratory (PAL, Republic of Korea), equipped with a Quantum 270 CCD detector (ADSC, USA). All data were indexed, integrated, and scaled together using the HKL2000 software package.[37] Crystals of *Nk*COMT belonged to the space group $P12_11$ with unit cell parameters a = 38.27 Å, b = 97.08 Å, c = 106.52 Å, $\alpha = \gamma = 90.0°$, and β = 93.4. With four molecules of *Nk*COMT in the asymmetric unit, the crystal volume per unit of protein mass was 2.05 $Å^3$ Da^{-1}, which indicates a solvent content of approximately 40.16%.[38] Crystals in complex with SAM belonged to the space group C_12_1 with unit cell parameters a = 166.18 Å, b = 93.18 Å, c = 43.34 Å, $\alpha = \gamma = 90.0°$, and β = 104.1. Assuming three molecules of *Nk*COMT per asymmetric unit, the crystal volume per unit of protein mass was 2.26 $Å^3$ Da^{-1}, which corresponds to a solvent content of approximately 45.52%.[38] Crystals in complex with SAH and Mg^{2+} belonged to the space group $P2_12_12_1$ with unit cell parameters a = 42.69 Å, b = 98.23 Å, c = 101.77 Å, and $\alpha = \beta = \gamma = 90.0°$. Assuming two molecules of *Nk*COMT per asymmetric unit, the crystal volume per unit of protein mass was 2.22 $Å^3$ Da^{-1}, which corresponds to a solvent content of approximately 44.61%.[38] All three structures of *Nk*COMT were determined by molecular replacement with the CCP4[39] version of MOLREP,[40] using the structure of COMT from *Streptomyces regensis* (PDB code 5N5D) as a search model. Further model building was performed manually using the program WinCoot,[40] and refinement was performed with CCP4 refmac5.[40] The refined models of *Nk*COMT, those in complex with SAM, and those in complex with SAH and Mg^{2+} were deposited in the Protein Data Bank with PDB codes of 7CVU, 7CVV, and 7CVW, respectively.[41]

Size-Exclusion Chromatographic (SEC) Analysis. Analytical size-exclusion chromatography was performed using a Superdex 200 10/300 GL column (GE Healthcare Life Sciences) with purified *Nk*COMT protein solution (2 mg/mL, 40 mM Tris-HCl pH 8.0, and 150 mM NaCl). The molecular mass of the eluted *Nk*COMT sample was calculated by a calibration curve. All experiments were performed in duplicate and at 277 K of column temperature.

RESULTS AND DISCUSSION

Metal Preference of *Nk*COMT. To investigate the biochemical properties of *Nk*COMT, we expressed and purified the *Nk*COMT protein by Ni-NTA and size-exclusion chromatography. It has been reported that Mg^{2+} is required for enzyme catalysis for most of the known OMTs, and other metal ions are required for a few enzymes. In order to investigate the metal preference of *Nk*COMT, we added 1 mM of various divalent metal ions, such as Mg^{2+}, Ca^{2+}, Mn^{2+}, Fe^{2+}, Ni^{2+}, Cu^{2+}, Zn^{2+}, Co^{2+}, and Cd^{2+}, to the EDTA-treated reaction mixtures containing protocatechuate (PCA) as a substrate (Figure 1A) and measured the enzyme activity by monitoring the amount of produced vanillic acid and *iso*-vanillic acid (Figure 1B). We detected a residual activity even without the addition of metal ions, indicating that a trace amount of metal ions remained in the protein despite EDTA treatment (Figure 1B). We observed the highest activity with Mg^{2+} among the divalent metal ions (Figure 1B). We also detected significant activities with Co^{2+}, Zn^{2+}, Cu^{2+}, and Cd^{2+}, and among these metal ions, Zn^{2+} and Cu^{2+} showed relatively higher activities (Figure 1B). We also measured the ratio of para- and meta-forms of the products. When Mg^{2+} was used, we observed the para- and meta-form

https://dx.doi.org/10.1021/acs.jafc.0c07621
J. Agric. Food Chem. 2021, 69, 2531−2538

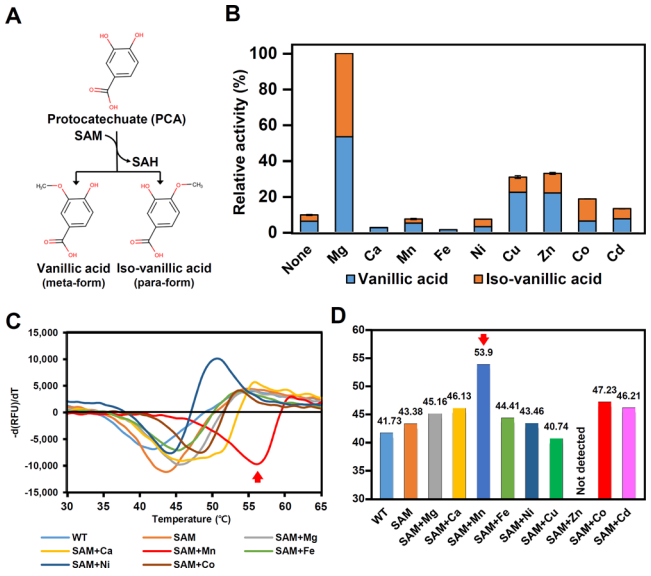

Figure 1. Metal preference of *Nk*COMT. (A) Enzymatic reaction of *Nk*COMT. (B) Metal preference of *Nk*COMT. The activities with various metal ions are shown based on that with Mg^{2+}. Each experiment was performed in triplicate. (C,D) Thermal stability of *Nk*COMT in the presence of metal ions. The highest increase in the T_m value was observed in the presence of Mn^{2+} and is indicated by a red-colored arrow.

products of the same ratio, and the reactions with Zn^{2+} and Cu^{2+} showed a higher ratio of meta- to para-form products (Figure 1B). These results indicate that the metal ion affects the meta- and para-regiospecificity of the enzyme as well as the enzyme activity.

Previous studies have shown that the binding affinity for ligands and metal ions is directly correlated with protein stabilization.[42,43] We then investigated how the metal ions affect the thermal stability of the *Nk*COMT enzyme. First, we investigated the effect of the addition of SAM on the thermal stability of *Nk*COMT, and the T_m values of the protein with and without addition of SAM were 43.38 and 41.73 °C, respectively (Figure 1C,D). These results suggest that the binding of SAM to *Nk*COMT increased the thermal stability of the enzyme. We then investigated how the addition of the metal ions affects the thermal stability of the enzyme. We observed increased T_m values by adding metal ions, such as Mg^{2+}, Ca^{2+}, Mn^{2+}, Fe^{2+}, Co^{2+}, and Cd^{2+}, and similar or lower T_m values by Ni^{2+} and Cu^{2+} (Figure 1C,D). In the case of Zn^{2+}, we could not measure the T_m value due to heavy precipitation. Interestingly, the most dramatic increase in the T_m value was observed with the addition of Mn^{2+} (Figure 1C,D). Based on these observations, we suggest that the metal preference for enzyme catalysis is not strongly correlated with the thermal stability of the enzyme/metal complex and consequently with the affinity of the enzyme for the metal ion.

Overall Structure of *Nk*COMT. In order to investigate the molecular mechanism of *Nk*COMT, we determined its structure in a ligand-free form at a 1.75 Å resolution. The refined structures have a good stereochemistry with the X-ray crystallographic statistics for the bond angle, bond lengths, and other geometric parameters (Table 1). The structure of *Nk*COMT adopts a Rossman fold similar to that of all conventional SAM-dependent COMTs (Figure 2A). The monomeric structure of *Nk*COMT forms a single domain and

Table 1. Data Collection and Refinement Statistics

parameter	*Nk*COMT_Apo	*Nk*COMT_SAM	*Nk*COMT _Mg^{2+} and SAH
Data collection			
space group	$P12_11$	C_12_1	$P2_12_12_1$
cell dimensions			
a, *b*, *c* (Å)	38.27, 97.08, 106.52	166.18, 93.18, 43.34	42.69, 98.23, 101.77
α, *β*, *γ* (°)	90.00, 93.38, 90.00	90.00, 104.12, 90.00	90.00, 90.00, 90.00
resolution (Å)	50.00−1.75 (1.78−1.75)	50.00−2.50 (2.54−2.50)	50.00−1.54 (1.57−1.54)
R_{sym}	8.2 (30.5)	12.6 (31.6)	7.9 (37.9)
I/σ (*I*)	30.3 (6.6)	32.6 (7.1)	34.5 (5.0)
completeness (%)	96.7 (96.4)	99.0 (98.2)	99.5 (99.1)
redundancy	3.7 (3.8)	5.4 (4.2)	6.2 (4.7)
Refinement			
resolution (Å)	50.00−1.75	50.00−2.50	50.00−1.54
no. of reflections	71,860	20,120	60,347
R_{work}/R_{free}	17.4 (21.0)	17.8 (21.8)	17.4 (19.5)
no. of atoms	7031	5110	3569
protein	6703	5016	3344
ligand/ion	12	81	66
water	316	13	159
B-factors	19.21	36.00	13.53
protein	20.68	39.00	14.50
ligand/ion	23.39	42.74	19.70
water	24.569	38.84	21.32
r.m.s. deviations			
bond lengths (Å)	0.0110	0.0072	0.0287
bond angles (°)	1.6347	1.5405	2.6630

consists of ten *α*-helices (*α*1−*α*10) and seven stranded *β*-sheets (*β*1−*β*7) surrounded by the *α*-helices. The active site is located in the loop region in the C-terminal direction of the *β*-sheet (Figure 2A).

When we performed analytical size-exclusion chromatography, *Nk*COMT eluted as a dimer with a molecular weight of approximately 48 kDa, indicating that the enzyme functions as a dimer (Figure 2B,C). PISA software, which calculated an oligomeric interface, calculated that an area of 1815.4 $Å^2$ of a solvent-accessible interface per monomer is buried, which constitutes 20.1% of the monomer solvent-accessible area.[44] The dimeric structure is mainly formed by hydrophobic interactions on the surface of four *α*-helices (*α*1, *α*3, *α*8, and *α*9) and two *β*-strands (*β*6 and *β*7), although some hydrophilic interactions also contribute to the formation of a dimer (Figure 2C).

SAM and Metal Ion Binding Mode of *Nk*COMT. To reveal the binding modes of the SAM cosubstrate and a metal ion, we determined the *Nk*COMT structures complexed with SAM and complexed with Mg^{2+} and *S*-adenosyl-L-homocysteine (SAH) at resolutions of 2.50 and 1.55 Å, respectively (Figure 3A,B and Table 1). Although we added SAM to the crystallization solution, we could not observe a clear electron density map for the methyl group (Figure 3A), indicating that the methyl group was released from the unstable SAM molecule during the crystallization procedure due to its chemical instability.[45] The SAM binding pocket is formed in the cavity

https://dx.doi.org/10.1021/acs.jafc.0c07621
J. Agric. Food Chem. 2021, 69, 2531−2538

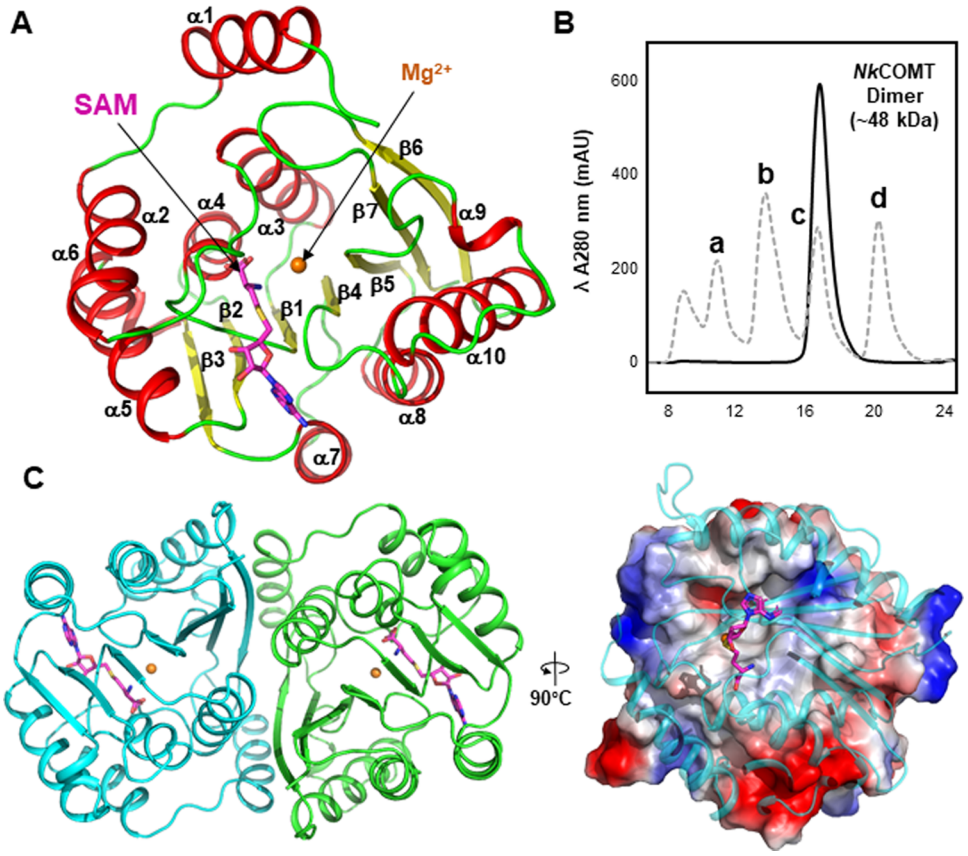

Figure 2. Overall structure of *Nk*COMT. (A) Monomeric structure of *Nk*COMT. The *Nk*COMT monomer structure is shown as a cartoon diagram, and its secondary structure elements are labeled. Bound SAH and Mg^{2+} are shown as a stick and sphere model with colors of magenta and orange, respectively. (B) Size-exclusion chromatography trace of *Nk*COMT. (a−d) indicate the standard samples of ferritin (440 kDa), conalbumin (75 kDa), carbonic anhydrase (29 kDa), and ribonuclease A (13.7 kDa). (C) Dimeric structure of *Nk*COMT. Two monomers are distinguished with colors of magenta and green. The right-side figure is rotated 90 degrees vertically from the left-side figure and presented with an electrostatic potential surface model for one molecule and a cartoon diagram for the other molecule.

at the C-terminal loop region of the five parallel β-sheets and is located on the surface (Figures 2A and 3C). Mg^{2+} is located in the vicinity of the methionine moiety of SAM and coordinated by the residues of Asp139, Asp165, and Asn166, and each distance from the residue to the metal ion is 2.4 Å (Figure 3D). Both the hydrophilic and hydrophobic residues are involved in the stabilization of the SAM molecule. The adenine moiety forms hydrogen bonds with and is stabilized by the side chains of Asp141 and Tyr148 and the main chains of Tyr90 and Ala118 (Figure 3D). The Tyr90 residue also forms a $\pi-\pi$ interaction with the adenine ring (Figure 3D). The two hydroxyl groups of the ribose ring form strong hydrogen bonds with the side chains of Glu89 and His94 and the main chain of Leu67 (Figure 3D). The side chains of residues Leu67 and Ile39 point in the direction of the substrate methyl group, and these two residues seem to form hydrophobic interactions with the methyl group of SAM (Figure 3D). The amine group of methionine is stabilized by the side chains of Ser71 and Asp139 and the main chain of Gly65 (Figure 3D). Finally, the carboxyl group of methionine forms hydrogen bonds with the main chains of Ser71 and Val41 (Figure 3D).

Conformational Changes upon Binding of SAM and the Metal Ion in *Nk*COMT. The structural analysis of the *Nk*COMT structures also shows that the protein undergoes conformational changes upon binding of the SAM substrate and Mg^{2+}. When we compared the ligand-free form and the SAM-complexed structures, the conformation of the $\alpha2-\alpha3$ connecting loop in the ligand-free form was significantly different from that in the SAM-complexed form (Figure 4A). The $\alpha2-\alpha3$ connecting loop is positioned away from the carboxyl group of SAM in the ligand-free form (Figure 4A). However, in the SAM-complexed structure, the loop moves to SAM. Consequently, the Val41 residue is located in the vicinity of SAM, allowing its main chain to form a hydrogen bond with the carboxyl group of SAM (Figure 4A). This structural movement also induces a conformational change in the $\beta6-\beta7$ connecting loop. The $\beta6-\beta7$ connecting loop does not interact with the $\alpha2-\alpha3$ connecting loop in the ligand-free form; however, in the SAM-complexed form, its conformation is changed to interact with the $\alpha2-\alpha3$ connecting loop (Figure 4A). In particular, the Lys210 residue forms a hydrogen bond with the main chain of Ser40 on the $\alpha2-\alpha3$ connecting loop (Figure 4A). We expected that these conformational changes might increase the stability of these loops, and in fact, the B-factor of the $\alpha2-\alpha3$ connecting loop in the SAM-complexed form was dramatically decreased compared to that in the ligand-free form (Figure 4B). When we compared the *Nk*COMT structure complexed with SAH/Mg^{2+} to the other structures of *Nk*COMT, the connecting loop of $\alpha2-\alpha3$ and $\beta6-\beta7$ showed conformations quite similar to those of the SAM-complexed structure (Figure 4A). In the complex structure with SAH/Mg^{2+}, we also observed the hydrogen bonds between the main chain of Val41 and the carboxyl group of SAM and between the side chain of Lys210 and the main chain of Ser40. Interestingly,

https://dx.doi.org/10.1021/acs.jafc.0c07621
J. Agric. Food Chem. 2021, 69, 2531−2538

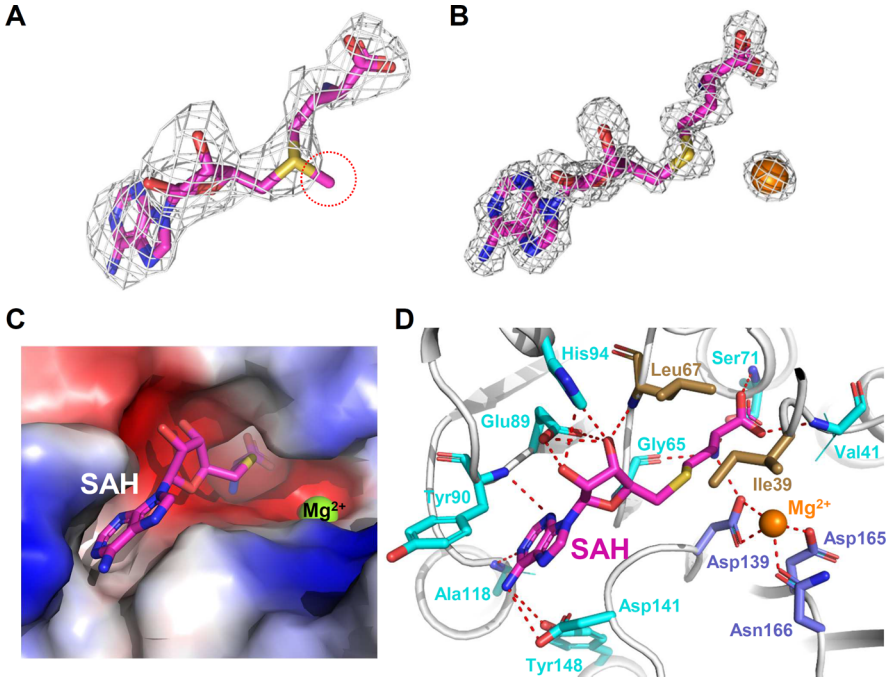

Figure 3. Binding modes of SAM and Mg^{2+} of *Nk*COMT. (A,B) Electron density maps of SAM (A) and SAH/Mg^{2+} (B). The Fo-Fc electron density maps of the bound ligands are shown with a gray-colored mesh with 2.0 σ contour. (C) SAM binding pocket. The *Nk*COMT structure is presented with an electrostatic potential surface model, and bound SAH and Mg^{2+} are shown as a stick and sphere model with colors of magenta and green, respectively. (D) SAM and Mg^{2+} binding modes. The residues involved in the binding of Mg^{2+} and SAH are shown in light-blue and cyan colors, respectively. The hydrophobic residues are shown in a dark-brown color.

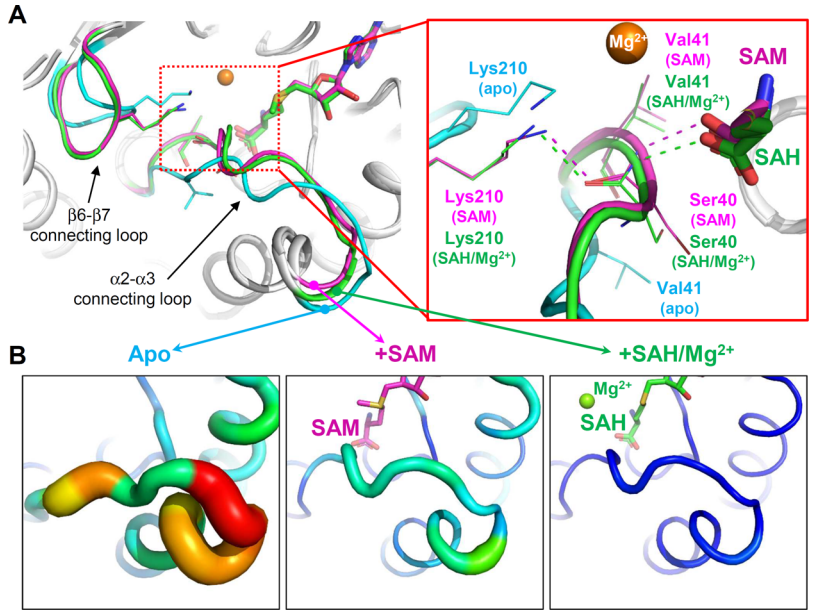

Figure 4. Conformational changes of *Nk*COMT upon cosubstrate and metal ion binding. (A) Conformational changes of *Nk*COMT. Three *Nk*COMT structures, a ligand-free form, a SAM complex, and a SAH Mg^{2+} complex, are presented with a cartoon diagram, and the regions that undergo conformational changes are distinguished with colors of cyan, magenta, and green, respectively. The magenta- and green-colored dotted lines indicate hydrogen bonds formed in the SAM-complexed form. (B) B-factor of the $\alpha2-\alpha3$ connecting loops. The *Nk*COMT structures are shown as a B-factor putty, and the $\alpha2-\alpha3$ connecting loops are zoomed.

however, the B-factor of the $\alpha2-\alpha3$ connecting loop in the SAH/Mg^{2+}-complexed form was decreased more than that in the SAM-complexed form (Figure 4B), indicating that the binding of Mg^{2+} makes the protein more stable. These observations are also consistent with previously described results that the addition of SAM and both SAM and Mg^{2+} enhanced the T_m values of the protein by 1.65 and 3.43 °C, respectively, compared to the protein alone.

Catechol Binding Mode of *Nk*COMT. To elucidate the substrate binding mode of *Nk*COMT, we attempted to determine the *Nk*COMT structure complexed with PCA, but neither cocrystallization nor soaking experiments were success-

https://dx.doi.org/10.1021/acs.jafc.0c07621
J. Agric. Food Chem. 2021, 69, 2531−2538

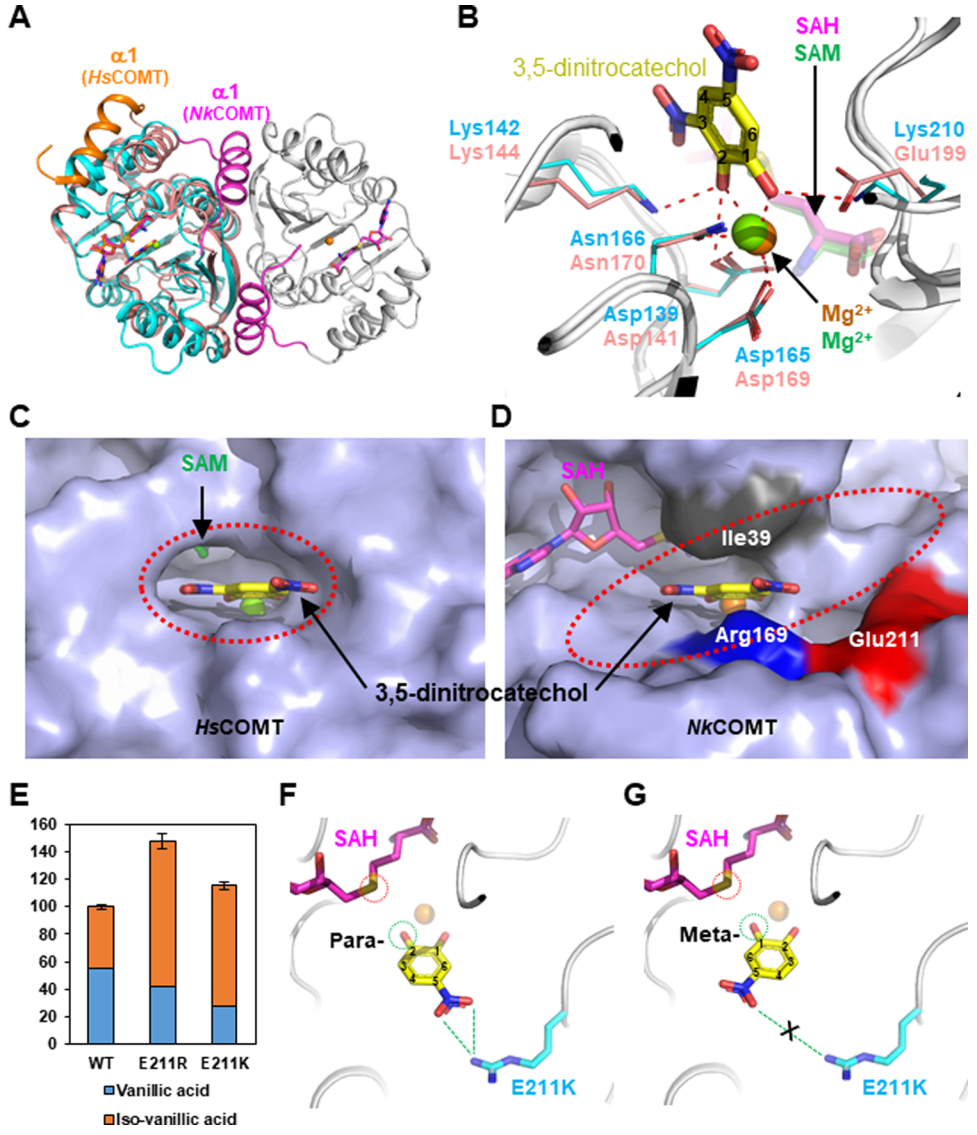

Figure 5. Regiospecificity of *Nk*COMT. (A) Superposition of structures of *Nk*COMT and *Hs*COMT. The *Nk*COMT structures are shown with cyan and gray colors for two different monomers, and the *Hs*COMT monomer is with a salmon color. The α1-helix of *Nk*COMT and *Hs*COMT is distinguished with colors of magenta and orange, respectively. (B) Catechol binding mode of *Nk*COMT. The *Nk*COMT structure complexed with SAH and Mg^{2+} is superposed with the *Hs*COMT structure complexed with 3,5-dinitrocatechol. The residues involved in the binding of Mg^{2+} and the two hydroxyl groups of catechol of *Nk*COMT and *Hs*COMT are shown as a line model with colors of cyan and salmon, respectively. (C,D) Catechol binding pocket of *Hs*COMT (C) and *Nk*COMT (D). The structures of *Hs*COMT and *Nk*COMT are presented with a light-blue-colored surface model. The catechol binding pocket is indicated with a red-colored dotted line. The bound catechol molecule in *Hs*COMT is shown as a yellow-colored stick model. The residues of Ile39, Arg168, and Glu211, located near the catechol molecule in *Nk*COMT, are shown in dark-gray, blue, and red, respectively. (E) Change of regiospecificity of *Nk*COMT. The activities of the variants shown on the basis of that of a wild type. Each experiment is performed in triplicate. (F,G) Structural basis for a changed regiospecificity. The figures are prepared by manually placing the PCA molecules in its binding pocket using PyMOL. The mutated E211K residue is shown as a stick model with a cyan color. The methyl-group position in SAM and the para- and meta-hydroxyl groups of PCA are indicated by red- and green-colored circles.

ful. Alternatively, we compared the SAH/Mg^{2+}-complexed *Nk*COMT structure to the structure of COMT from *Homo sapiens* (*Hs*COMT) complexed with the 3,5-dinitrocatechol (DNC) inhibitor (PDB code 6I3C). Although these two enzymes showed quite similar overall structures to each other, *Hs*COMT exists as a monomer, unlike *Nk*COMT that forms a dimer (Figure 5A). The difference in the oligomeric status of these two enzymes seems to be due to a difference in the position of the α1-helix (Figure 5A). The position of Mg^{2+} and the residues involved in stabilizing the metal in *Hs*COMT is almost identical to those of *Nk*COMT, indicating that these two enzymes catalyze the enzyme reaction in a way similar to each other (Figure 5B). However, the catechol binding modes of these two enzymes are somewhat different from each other. In *Hs*COMT, Glu199 and Lys144 residues form hydrogen bonds with the 1′- and 2′-hydroxyl groups of DNC, respectively (Figure 5B). In *Nk*COMT, two lysine residues, Lys142 and Lys210, are located at the corresponding positions of Glu199 and Lys144 in *Hs*COMT (Figure 5B). Nevertheless, these observations led us to speculate that *Nk*COMT might accommodate the catechol substrates in a way similar to *Hs*COMT. Surprisingly, however, the catechol ring binding pockets of these two enzymes are substantially different from each other; whereas the binding pocket of *Hs*COMT is narrow

https://dx.doi.org/10.1021/acs.jafc.0c07621
J. Agric. Food Chem. 2021, 69, 2531−2538

and is able to accommodate only small catechol substrates, *Nk*COMT shows a widely open substrate binding pocket (Figure 5C,D). These observations might explain how bacterial COMTs have a broad substrate specificity and utilize catechol derivatives with multicyclic structures as substrates. For the stabilization of the PCA substrate, the Ile39 residue forms hydrophobic interactions with the catechol ring, and the Arg169 residue interacts with the 5′-carboxyl group (Figure 5D).

Selection of Regiospecificity of *Nk*COMT. It has been known that most of the COMTs do not have a regiospecificity and produce both the meta- and para-forms of the products. As we have described above, *Nk*COMT also does not have a regiospecificity, thus producing the meta- and para-forms of the products in equal proportion. We then attempted to develop *Nk*COMT variants having a regiospecificity for the substrate. We designed to replace the Glu211 residue with arginine or lysine, expecting that the mutated arginine or lysine residue might form a salt bridge with the 5′-carboxyl group of PCA. Interestingly, both *Nk*COMT^{E211R} and *Nk*COMT^{E211K} variants showed an enhanced activity compared with a wild type, and moreover, the ratio of *iso*-vanillic acid and vanillic acid was dramatically increased from both variants (Figure 5E). We propose that the mutated arginine or lysine residues stabilize the 5′-carboxyl group of PCA and consequently place the PCA substrate to the orientation that allows the methyl group to be transferred to the para-hydroxyl group (Figure 5F,G). Moreover, both the *Nk*COMT^{E211R} and the *Nk*COMT^{E211K} variants showed enhanced activities by approximately 50 and 20%, respectively, compared with a wild type (Figure 5E). Also, we suggest that the additional involvement of the introduced positively charged arginine or lysine residues increased the substrate affinity to the enzyme.

In summary, we analyzed the biochemical properties and metal preference of *Nk*COMT and determined the first crystal structure of *Nk*COMT. We also determined the complex structures with SAM and SAH/Mg^{2+} and elucidated the binding modes of Mg^{2+} and the SAM substrate. Based on structural information of the apo and complexed structures, we also revealed that the region near the SAM binding site undergoes conformational changes upon the binding of SAM and Mg^{2+}. Finally, we identified the binding pocket of the PCA substrate and explained how the bacterial enzymes accommodate the catechol compounds of various sizes, for example, multicyclic catechol, as a substrate. In addition, we developed the *Nk*COMT variants that show enhanced regiospecificity, resulting in a higher proportion of the para-form of products than the meta-form. From this perspective, mutations near the substrate binding site can remarkably influence the control of regiospecificity.

AUTHOR INFORMATION

Corresponding Author

Kyung-Jin Kim − *School of Life Sciences, KNU Creative BioResearch Group, Kyungpook National University, Daegu 41566, Republic of Korea; KNU Institute for Microorganisms, Kyungpook National University, Daegu 41566, Republic of Korea;* orcid.org/0000-0002-0375-2561; Phone: +82-53-950-5377; Email: kkim@knu.ac.kr; Fax: +82-53-955-5522

Authors

Seul Hoo Lee − *School of Life Sciences, KNU Creative BioResearch Group, Kyungpook National University, Daegu 41566, Republic of Korea; KNU Institute for Microorganisms, Kyungpook National University, Daegu 41566, Republic of Korea*

Bongsang Kim − *School of Life Sciences, KNU Creative BioResearch Group, Kyungpook National University, Daegu 41566, Republic of Korea; KNU Institute for Microorganisms, Kyungpook National University, Daegu 41566, Republic of Korea*

Complete contact information is available at: https://pubs.acs.org/10.1021/acs.jafc.0c07621

Author Contributions

#S.H.L. and B.K. contributed equally to this work.

Author Contributions

The authors have made the following declarations about their contributions: K.-J.K. conceived and designed the experiments. B.K. and S.H.L. performed the experiments. B.K. and S.H.L. analyzed the data. S.H.L. and K.-J.K. wrote the paper.

Notes

The authors declare no competing financial interest.

ACKNOWLEDGMENTS

This research was supported by the Bio & Medical Technology Development Program of the National Research Foundation (NRF) funded by the Ministry of Science & ICT (NRF-2020M3A9I5037635) of the Republic of Korea.

REFERENCES

(1) Liscombe, D. K.; Louie, G. V.; Noel, J. P. Architectures, mechanisms and molecular evolution of natural product methyltransferases. *Nat. Prod. Rep.* **2012**, *29*, 1238−1250.

(2) Struck, A. W.; Thompson, M. L.; Wong, L. S.; Micklefield, J. S-Adenosyl-Methionine-Dependent Methyltransferases: Highly Versatile Enzymes in Biocatalysis, Biosynthesis and Other Biotechnological Applications. *ChemBioChem* **2012**, *13*, 2642−2655.

(3) Jaeck, E.; Martz, F.; Stiefel, V.; Fritig, B.; Legrand, M. Expression of class I O-methyltransferase in healthy and TMV-infected tobacco. *Mol. Plant-Microbe Interact.* **1996**, *9*, 681−688.

(4) Nikodejevic, B.; Senoh, S.; Daly, J. W.; Creveling, C. R. Catechol-O-methyltransferase. II. A new class of inhibitors of catechol-o-methyltransferase; 3,5-dihydroxy-4-methoxybenzoic acid and related compounds. *J Pharmacol Exp Ther* **1970**, *174*, 83−93.

(5) Lee, S.; Kang, J.; Kim, J. Structural and biochemical characterization of Rv0187, an O-methyltransferase from Mycobacterium tuberculosis. *Sci. Rep.* **2019**, *9*, 8059.

(6) Weinshilboum, R. M.; Otterness, D. M.; Szumlanski, C. L. Methylation pharmacogenetics: catechol O-methyltransferase, thiopurine methyltransferase, and histamine N-methyltransferase. *Annu. Rev. Pharmacol. Toxicol.* **1999**, *39*, 19−52.

(7) Chatterjee, D.; Kudlinzki, D.; Linhard, V.; Saxena, K.; Schieborr, U.; Gande, S. L.; Wurm, J. P.; Wöhnert, J.; Abele, R.; Rogov, V. V.; Dotsch, V.; Osiewacz, H. D.; Sreeramulu, S.; Schwalbe, H. Structure and Biophysical Characterization of the S-Adenosylmethionine-dependent O-Methyltransferase PaMTH1, a Putative Enzyme Accumulating during Senescence of Podospora anserina. *J. Biol. Chem.* **2015**, *290*, 16415−16430.

(8) Yan, Q.; Shaw, N.; Qian, L.; Jiang, D. Crystal structure of Rv1220c, a SAM-dependent O-methyltransferase from Mycobacterium tuberculosis. *Acta Crystallogr F Struct Biol Commun* **2017**, *73*, 315−320.

(9) Hou, X.; Wang, Y.; Zhou, Z.; Bao, S.; Lin, Y.; Gong, W. Crystal structure of SAM-dependent O-methyltransferase from pathogenic bacterium Leptospira interrogans. *J. Struct. Biol.* **2007**, *159*, 523−528.

(10) Kilgore, M. B.; Augustin, M. M.; Starks, C. M.; O'Neil-Johnson, M.; May, G. D.; Crow, J. A.; Kutchan, T. M. Cloning and characterization of a norbelladine 4'-O-methyltransferase involved in

the biosynthesis of the Alzheimer's drug galanthamine in Narcissus sp. aff. pseudonarcissus. *PLoS One* **2014**, *9*, No. e103223.
(11) Kopycki, J. G.; Stubbs, M. T.; Brandt, W.; Hagemann, M.; Porzel, A.; Schmidt, J.; Schliemann, W.; Zenk, M. H.; Vogt, T. Functional and structural characterization of a cation-dependent O-methyltransferase from the cyanobacterium Synechocystis sp. strain PCC 6803. *J. Biol. Chem.* **2008**, *283*, 20888−20896.
(12) Nelson, J. T.; Lee, J.; Sims, J. W.; Schmidt, E. W. Characterization of SafC, a catechol 4-O-methyltransferase involved in saframycin biosynthesis. *Appl. Environ. Microbiol.* **2007**, *73*, 3575−3580.
(13) Axelrod, J.; Tomchick, R. Enzymatic O-methylation of epinephrine and other catechols. *J. Biol. Chem.* **1958**, *233*, 702−705.
(14) Bonifácio, M. J.; Archer, M.; Rodrigues, M. L.; Matias, P. M.; Learmonth, D. A.; Carrondo, M. A.; Soares-Da-Silva, P. Kinetics and crystal structure of catechol-o-methyltransferase complex with co-substrate and a novel inhibitor with potential therapeutic application. *Mol. Pharmacol.* **2002**, *62*, 795−805.
(15) Czarnota, S.; Johannissen, L. O.; Baxter, N. J.; Rummel, F.; Wilson, A. L.; Cliff, M. J.; Levy, C. W.; Scrutton, N. S.; Waltho, J. P.; Hay, S. Equatorial Active Site Compaction and Electrostatic Reorganization in Catechol-O-methyltransferase. *ACS Catal.* **2019**, *9*, 4394−4401.
(16) Iijima, H.; Takebe, K.; Suzuki, M.; Kobayashi, H.; Takamiya, T.; Saito, H.; Niwa, N.; Kuwada-Kusunose, T. Crystal Structure of Catechol O-Methyltransferase Complexed with Nitecapone. *Chem. Pharm. Bull.* **2020**, *68*, 447−451.
(17) Lerner, C.; Ruf, A.; Gramlich, V.; Masjost, B.; Zürcher, G.; Jakob-Roetne, R.; Borroni, E.; Diederich, F. X-ray Crystal Structure of a Bisubstrate Inhibitor Bound to the Enzyme Catechol-O-methyltransferase: A Dramatic Effect of Inhibitor Preorganization on Binding Affinity We thank F. Hoffmann-La Roche for generous support of this work. We are grateful to P. Malherbe for the cloning of COMT, P. Caspers for the expression of COMT, A. Cesura for enzyme purification, B. Wipf for fermentation, and H. W. Lahm for sequencing. *Angew. Chem., Int. Ed. Engl.* **2001**, *40*, 4040−4042.
(18) Vidgren, J.; Svensson, L. A.; Liljas, A. Crystal structure of catechol O-methyltransferase. *Nature* **1994**, *368*, 354−358.
(19) Ehler, A.; Benz, J.; Schlatter, D.; Rudolph, M. G. Mapping the conformational space accessible to catechol-O-methyltransferase. *Acta Crystallogr. D Biol. Crystallogr.* **2014**, *70*, 2163−2174.
(20) Walker, A. M.; Sattler, S. A.; Regner, M.; Jones, J. P.; Ralph, J.; Vermerris, W.; Sattler, S. E.; Kang, C. The Structure and Catalytic Mechanism of Sorghum bicolor Caffeoyl-CoA O-Methyltransferase. *Plant Physiol.* **2016**, *172*, 78−92.
(21) Yager, J. D. Catechol-O-methyltransferase: characteristics, polymorphisms and role in breast cancer. *Drug. Discov. Today: Dis. Mech.* **2012**, *9*, e41−e46.
(22) Zhong, R.; Morrison, W. H., III; Himmelsbach, D. S.; Poole, F. L., II; Ye, Z. H. Essential role of caffeoyl coenzyme A O-methyltransferase in lignin biosynthesis in woody poplar plants. *Plant Physiol.* **2000**, *124*, 563−578.
(23) Kunjapur, A. M.; Prather, K. L. J. Development of a Vanillate Biosensor for the Vanillin Biosynthesis Pathway in E. coli. *ACS Synth. Biol.* **2019**, *8*, 1958−1967.
(24) Kim, H. T.; Kim, J. K.; Cha, H. G.; Kang, M. J.; Lee, H. S.; Khang, T. U.; Yun, E. J.; Lee, D. H.; Song, B. K.; Park, S. J.; Joo, J. C.; Kim, K. H. Biological Valorization of Poly(ethylene terephthalate) Monomers for Upcycling Waste PET. *ACS Sustainable Chem. Eng.* **2019**, *7*, 19396−19406.
(25) Ferrer, J. L.; Zubieta, C.; Dixon, R. A.; Noel, J. P. Crystal structures of alfalfa caffeoyl coenzyme A 3-O-methyltransferase. *Plant Physiol.* **2005**, *137*, 1009−1017.
(26) Haydock, S. F.; Appleyard, A. N.; Mironenko, T.; Lester, J.; Scott, N.; Leadlay, P. F. Organization of the biosynthetic gene cluster for the macrolide concanamycin A in Streptomyces neyagawaensis ATCC 27449. *Microbiology* **2005**, *151*, 3161−3169.
(27) Hara, O.; Hutchinson, C. R. A macrolide 3-O-acyltransferase gene from the midecamycin-producing species Streptomyces mycarofaciens. *J. Bacteriol.* **1992**, *174*, 5141−5144.
(28) Pospiech, A.; Bietenhader, J.; Schupp, T. Two multifunctional peptide synthetases and an O-methyltransferase are involved in the biosynthesis of the DNA-binding antibiotic and antitumour agent saframycin Mx1 from Myxococcus xanthus. *Microbiology* **1996**, *142*, 741−746.
(29) von Tesmar, A.; Hoffmann, M.; Pippel, J.; Fayad, A. A.; Dausend-Werner, S.; Bauer, A.; Blankenfeldt, W.; Müller, R. Total Biosynthesis of the Pyrrolo[4,2]benzodiazepine Scaffold Tomaymycin on an In Vitro Reconstituted NRPS System. *Cell Chem. Biol.* **2017**, *24*, 1216−1227.e8.
(30) Law, B. J. C.; Bennett, M. R.; Thompson, M. L.; Levy, C.; Shepherd, S. A.; Leys, D.; Micklefield, J. Effects of Active-Site Modification and Quaternary Structure on the Regioselectivity of Catechol-O-Methyltransferase. *Angew. Chem., Int. Ed. Engl.* **2016**, *55*, 2683−2687.
(31) Männistö, P. T.; Kaakkola, S. Catechol-O-methyltransferase (COMT): biochemistry, molecular biology, pharmacology, and clinical efficacy of the new selective COMT inhibitors. *Pharmacol. Rev.* **1999**, *51*, 593−628.
(32) Chávez, A. S. O.; Fairman, J. W.; Felsheim, R. F.; Nelson, C. M.; Herron, M. J.; Higgins, L.; Burkhardt, N. Y.; Oliver, J. D.; Markowski, T. W.; Kurtti, T. J.; Edwards, T. E.; Munderloh, U. G. An O-Methyltransferase Is Required for Infection of Tick Cells by Anaplasma phagocytophilum. *PLoS Pathog.* **2015**, *11*, e1005248.
(33) Franklin, M. C.; Cheung, J.; Rudolph, M. J.; Burshteyn, F.; Cassidy, M.; Gary, E.; Hillerich, B.; Yao, Z. K.; Carlier, P. R.; Totrov, M.; Love, J. D. Structural genomics for drug design against the pathogen Coxiella burnetii. *Proteins* **2015**, *83*, 2124−2136.
(34) Siegrist, J.; Netzer, J.; Mordhorst, S.; Karst, L.; Gerhardt, S.; Einsle, O.; Richter, M.; Andexer, J. N. Functional and structural characterisation of a bacterial O-methyltransferase and factors determining regioselectivity. *FEBS Lett.* **2017**, *591*, 312−321.
(35) Lee, S. H.; Son, H. F.; Kim, K. J. Structural insights into the inhibition properties of archaeon citrate synthase from Metallosphaera sedula. *PLoS One* **2019**, *14*, e0212807.
(36) Lee, S. H.; Kim, K. J. Crystal structure and biochemical properties of msed_0281, the citrate synthase from Metallosphaera sedula. *Biochem. Biophys. Res. Commun.* **2019**, *509*, 722−727.
(37) Otwinowski, Z.; Minor, W. [20] Processing of X-ray diffraction data collected in oscillation mode. *Methods Enzymol.* **1997**, *276*, 307−326.
(38) Chruszcz, M.; Potrzebowski, W.; Zimmerman, M. D.; Grabowski, M.; Zheng, H.; Lasota, P.; Minor, W. Analysis of solvent content and oligomeric states in protein crystals - does symmetry matter? *Protein Sci.* **2008**, *17*, 623−632.
(39) Collaborative Computational Project Number 4. The CCP4 suite: programs for protein crystallography. *Acta Crystallogr. D Biol. Crystallogr.* **1994**, *50*, 760−763.
(40) Vagin, A.; Teplyakov, A. Molecular replacement with MOLREP. *Acta Crystallogr. D* **2010**, *66*, 22−25.
(41) The Protein Data Bank. *Comput. Sci. Eng.* **2010**, *12* (), 10−10.
(42) Matulis, D.; Kranz, J. K.; Salemme, F. R.; Todd, M. J. Thermodynamic stability of carbonic anhydrase: measurements of binding affinity and stoichiometry using ThermoFluor. *Biochemistry* **2005**, *44*, 5258−5266.
(43) Zheng, L.; Hogue, C. W. V.; Brennan, J. D. Effects of metal binding affinity on the chemical and thermal stability of site-directed mutants of rat oncomodulin. *Biophys. Chem.* **1998**, *71*, 157−172.
(44) Krissinel, E.; Henrick, K. Inference of macromolecular assemblies from crystalline state. *J. Mol. Biol.* **2007**, *372*, 774−797.
(45) Morana, A.; Stiuso, P.; Colonna, G.; Lamberti, M.; Cartenì, M.; De Rosa, M. Stabilization of S-adenosyl-L-methionine promoted by trehalose. *Bba-Gen Subjects* **2002**, *1573*, 105−108.

https://dx.doi.org/10.1021/acs.jafc.0c07621
J. Agric. Food Chem. 2021, 69, 2531−2538